

Unsupervised Cross-Domain 3D Human Pose Estimation via Pseudo-Label-Guided Global Transforms

Jingjing Liu, Zhiyong Wang, Xinyu Fan, Amirhossein Dadashzadeh, Honghai Liu, *Fellow, IEEE*, Majid Mirmehdi

Abstract—Existing 3D human pose estimation methods often suffer in performance, when applied to cross-scenario inference, due to domain shifts in characteristics such as camera viewpoint, position, posture, and body size. Among these factors, camera viewpoints and locations have been shown to contribute significantly to the domain gap by influencing the global positions of human poses. To address this, we propose a novel framework that explicitly conducts global transformations between pose positions in the camera coordinate systems of source and target domains. We start with a Pseudo-Label Generation Module that is applied to the 2D poses of the target dataset to generate pseudo-3D poses. Then, a Global Transformation Module leverages a human-centered coordinate system as a novel bridging mechanism to seamlessly align the positional orientations of poses across disparate domains, ensuring consistent spatial referencing. To further enhance generalization, a Pose Augmentor is incorporated to address variations in human posture and body size. This process is iterative, allowing refined pseudo-labels to progressively improve guidance for domain adaptation. Our method is evaluated on various cross-dataset benchmarks, including Human3.6M, MPI-INF-3DHP, and 3DPW. The proposed method outperforms state-of-the-art approaches and even outperforms the target-trained model.

Index Terms—3D human pose estimation, domain adaptation, pseudo-label, global.

I. INTRODUCTION

HUMAN pose estimation has a wide range of applications, including video surveillance [1] [2], augmented reality [3]–[5], motion analysis [6] [7], robotics [8] [9], and human-computer interaction [10] [11]. While current methods for 3D human pose estimation have made significant progress, acquiring large amounts of diverse 3D data remains a major challenge. Most existing approaches [12]–[15] rely on datasets collected in controlled laboratory environments, while the variability of data is often limited. As a result, when these models are applied to other significantly different scenarios, their performances tend to degrade due to the lack of diversity in the training data. This highlights the need to tackle the challenges of achieving adaptability in different scenarios.

The domain gap in 3D human pose estimation typically arises from factors such as camera viewpoint, human postures, actions, and even body sizes [16]–[19]. To address such

This work was supported by the TORUS Project, which has been funded by the UK Engineering and Physical Sciences Research Council (EPSRC), grant number EP/X036146/1.

J. Liu (Corresponding author), A. Dadashzadeh and M. Mirmehdi are with the School of Computer Science, University of Bristol, United Kingdom. (e-mail: jingjing.liu@bristol.ac.uk)

Z. Wang and H. Liu are with the State Key Laboratory of Robotics and Systems, Harbin Institute of Technology Shenzhen, China.

Xinyu Fan is with the School of Aerospace Engineering, Xiamen University, China.

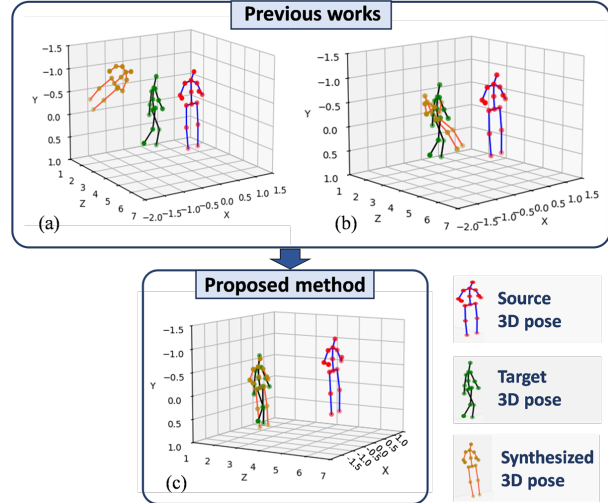


Fig. 1. Addressing the domain gap over camera viewpoints and locations. Rigid transformation operations (rotation and translation) are used to control pose adaptation to variations in camera viewpoints and positions. Most previous works synthesized data from source 3D poses through (a) randomly initialized rotation and translation within adversarial learning and (b) explicit computation of the translation matrices that still relied on randomly initialized rotation matrices within adversarial learning. In our method, (c) we propose explicit computation of both the rotation and translation matrices to align the source and target data.

shortcomings, previous methods have focused mainly on data augmentation via adversarial training to increase the diversity of source data, and incorporate the augmented poses in pose estimation model training [17], [18], [20]. For example, [17] and [18] explored different ways of designing a differentiable pose augmentor that learned to change various types of factors such as the bone angle, bone length, and rigid transformation of the whole pose (rotation and translation), with [17] dealing with a single pose and [18] dealing with a pose sequence. More recently, in [20] two pose augmentors were used combined with meta-optimization to ensure the preservation of source-specific information while simultaneously exploring out-of-source distributions. However, the data augmentation process in [17], [18], [20] relied on randomly initialized GAN-based adversarial training (see Fig. 1 (a)) that only captures the source data distributions. Moreover, the discriminator in their GANs enhanced similarity between augmented and source data, so these methods were restricted to explore out-of-source distributions. Therefore, when target poses significantly deviate from the source distributions, these methods fail to address the domain gap efficiently.

To effectively generate poses that simulate the target domain, it is crucial to exploit the knowledge embedded in the

target dataset. However, this aspect remains heavily under-explored, with only [21] and [22] as works of significance. For example, to address the large distribution gap due to camera positions, [21] exploited the direct use of the camera’s intrinsic parameters in the computation of the transformation operation between the source and target poses. The translation matrices for human poses were explicitly calculated, while the rotations were obtained through a GAN-based augmentor (see Fig. 1 (b)) that also considered bone vector and bone length. In [22], a diffusion based model was applied to generate multiple 3D pose hypotheses, using target 2D poses for conditioning, to simulate the 3D pose distribution in the target domain. Despite their attempts, [21] and [22] do not fully leverage the latent knowledge of the target dataset and cannot ensure that the generated data remains as consistent as possible with the target dataset.

In this paper, we address the domain discrepancy in 3D human pose estimation, predicated on camera viewpoints and positions, by aligning the 3D poses between the source and target camera coordinate systems through a target-domain-driven global transformation. Here, the global transformation refers to the transformation between absolute coordinates under camera coordinate systems rather than root-relative coordinates such that 2D poses can also be aligned after camera projection. Compared with augmenting rotation and translation matrices through GAN-based adversarial learning in which the parameters are randomly initialized as shown in Fig. 1(a), our target-driven global transformation is more intuitive and effective in adapting to camera viewpoints and positions (see Fig. 1(c)). The explicit computation of rotation and translation matrices make the synthesized data align with the source data in space as closely as possible.

Given the 2D poses of the target dataset, we propose a Pseudo-Label Generation Module to generate 3D poses as pseudo-labels by applying constraints based on human bone length or pre-trained models [23] [24]. Next, to align 3D poses between the source and target domains, we introduce a novel human body-centered coordinate system, which serves as a bridge in the rotation and translation process. Then the aligned 3D poses from the source dataset are projected into 2D using the camera intrinsic parameters of the target domain, resulting in aligned 2D poses as well. In addition to addressing variations of camera viewpoint and position, we incorporate a GAN-based Pose Augmentor to handle human posture and body size differences. The Pose Augmentor generates sequences of 3D human poses by changing bone angles and lengths. These sequences and corresponding reprojected 2D pose sequences are subsequently fed into two discriminators to refine them for better fidelity. Finally, these synthesized 2D-3D data pairs are used to fine-tune a pre-trained 3D pose estimation model. At each iteration, the pose estimator generates increasingly more accurate pseudo-labels to better adapt to the target domain.

Our main contributions can be summarized as follows: (i) We propose a novel global transformation method to reduce the domain discrepancies caused by varying camera parameters. This approach is significantly resilient to camera position and viewpoint variations, without introducing any

additional training parameters. (ii) We leverage the target dataset’s latent knowledge by utilizing its pseudo-labels to guide data synthesis, approximating its underlying distributions. (iii) We demonstrate the effectiveness and efficiency of the proposed method through experiments and ablations on three benchmarks, Human3.6M (H36M), MPI-INF-3DHP (3DHP) and 3DPW and achieve state-of-the-art results on H36M-3DHP and H36M-3DPW cross-dataset evaluation, outperforming the latest state-of-the-art method by 7.2% and 11.8% respectively. Our cross-dataset evaluation results in an unsupervised setting on the target dataset even surpass the target-specific trained MixSTE model [24]. Additionally, we simulate a new viewpoint based on the 3DHP dataset to further validate the robustness of our method.

II. RELATED WORK

A. 3D Human Pose Estimation

Recent years have seen significant advances in skeleton-based 3D human pose estimation, which can be categorized into two primary approaches: (a) One-stage methods, such as [25], [26], [27], and [28], which directly predict 3D poses from input images or videos, and (b) Two-stage methods, exemplified by [29], [30], [31], and [32], which first estimate 2D poses from images or videos [33]–[35] and subsequently lift these to 3D. Martinez et al. [36] conducted pioneering work demonstrating that lifting ground truth 2D joint positions to 3D can be accomplished with very low errors. As 2D pose estimation techniques are quite mature [37]–[39], therefore here we will only focus on mainly recent methods that lift 2D poses to 3D.

PoseFormer [29] was the first purely transformer-based 3D pose estimation approach in which a spatial transformer encoded the local relationships between the 2D joints and a temporal transformer captured global dependencies across the arbitrary frames. Later, Zhang et al. [24] proposed MixSTE which had spatial and temporal transformers performing alternately to enhance feature encoding for 3D pose estimation.

More recently, diffusion models have been explored to generate multi-hypotheses for 3D pose estimation, e.g. [40] [41]. These often involve a learned reverse process where noise is removed step-by-step to recover the true pose. Shan et al. [40] proposed a joint-level aggregation method based on reprojection errors from multiple hypotheses and achieved exceptional performance. Rather than directly regressing the 3D joint coordinates as in [40], the work in [41] decomposed the 3D pose into bone length and direction in the forward diffusion process to speed up gradient descent. Although these methods perform well on their training dataset, their performance tends to degrade when generalized to other datasets [20], [22].

B. Data augmentation on 3D human poses

To improve the generalisation ability of a model, previous approaches used data augmentation to increase the diversity of training data [17], [18], [20], [42]–[46]. Some methods [42] [43] focused on augmenting the original images, but more relevant to our method are those that enhanced 2D-3D pose pairs [17], [18], [20], [45]–[47]. Commonly in the

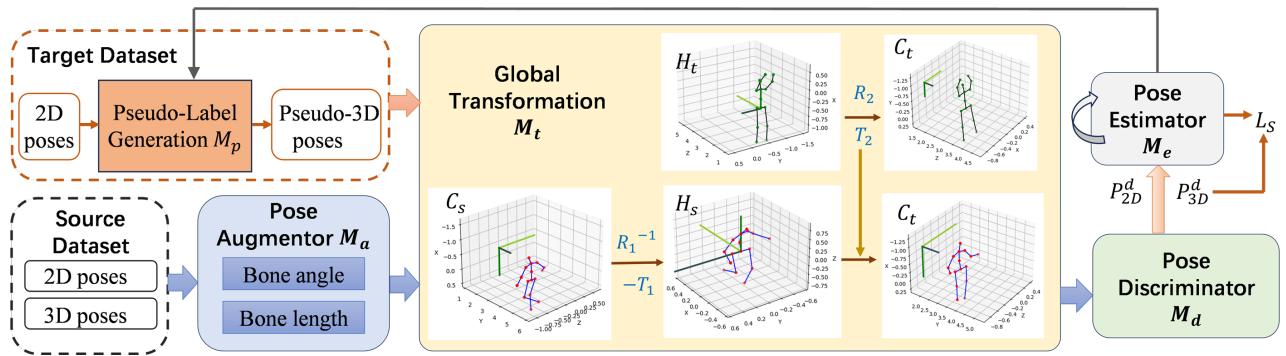


Fig. 2. **Overview of the proposed method.** The pseudo-3D poses from target dataset are used to guide the global transformation of the augmented 3D poses from source dataset. During the transformation, a human-centric coordinate system is proposed as a bridge. The synthesized 2D-3D pose pairs are then used to train the Discriminator M_d and Pose Estimator M_e jointly. The fine-tuned Pose Estimator helps generate more accurate pseudo-3D poses of the target dataset, making the framework iterative.

latter methods, the data augmentor is jointly trained with the discriminator and the pose estimator end-to-end with an error-feedback training strategy. As such, the augmentor learns to augment data with guidance from the estimator and discriminator in an unsupervised way (also see Section II-C). The augmented data are used to train the pose estimator, thus improving generalization and adaption ability of the pose estimator. For example, in PoseAug [17], data augmentation was applied in terms of bone angles, lengths, and body rigid transformations. More recently, Peng et al. [20] proposed a dual-augmentor framework, which included both a weak and a strong pose augmentor. This approach preserved knowledge of source poses while exploring out-of-source distributions. [47] proposed a Biomechanical Pose Generator (BPG), a novel approach that harnessed biomechanical principles, particularly the normal range of motion, to autonomously generate diverse and realistic 3D poses. This approach did not rely on the source dataset, thus overcoming the restrictions of popularity bias.

C. Unsupervised Domain Adaptation in 3D Pose Estimation

Unsupervised domain adaptation in 3D human pose estimation involves transferring models from the fully labeled source domain to an unlabeled target domain, with several different strategies seen in recent works. Zhang et al. [16] proposed an Inference Stage Optimization which performed geometry-aware self-supervised learning (SSL) on each single target instance and updated the 3D pose model before making predictions. Guan et al. [48] used 2D information of individual test frames and temporal constraints to fine-tune the source model on test video streams.

Recently, some works have aimed to further improve performance by synthesizing data from the source dataset in other ways [21], [22]. The synthesized data are typically designed to match the distribution of the target domain, and then used to train the pose estimator, to improve its adaption ability. For example, to address the domain gap in camera viewpoints, Chai et al. [21] exploited geometric constraints to align the root joint positions of 3D poses between the source and target domains. They also aligned the scales and root positions of 2D poses from the source and target domain using the target

camera intrinsic parameters. Furthermore, they incorporated the state-of-the-art human pose estimator based on a diffusion model, i.e., D3DP [40], to generate pseudo 2D-3D pairs of the target domain [22]. Although these methods attempt to simulate the target domain, their exploration of the latent knowledge within the target domain remains insufficient or inefficient and does not guarantee the consistency between the generated data and the target dataset. This gap highlights the need for more effective methods to extract and utilize target domain knowledge to better simulate the target domain.

Next, we introduce a method that proposes global transformations to address the variations in camera viewpoints and positions, which are key contributors to the domain gap [17] [18]. Guided by the target domain, our approach aims to align both 2D and 3D poses between the source and target domains to match the target data distribution as closely as possible. The proposed method integrates a Global Transformation module with a Pose Augmentor that augments bone angles and lengths. This combination achieves state-of-the-art performance in cross-domain 3D human pose estimation tasks.

III. METHOD

A. Problem Formulation

Unsupervised cross-domain 3D human pose estimation aims to adapt a pose estimation model trained on a labeled source dataset to an unlabeled target dataset. Let the human pose representation consist of J skeleton joints, numbered from 0 to $J - 1$ (see Fig. 3 where $J = 16$). We define $\mathbf{P}_{2D}^{src} \in \mathbb{R}^{2 \times J}$ to denote the 2D pose and $\mathbf{P}_{3D}^{src} \in \mathbb{R}^{3 \times J}$ to denote the label, i.e., a 3D pose from the source dataset and, $\mathbf{P}_{2D}^{tgt} \in \mathbb{R}^{2 \times J}$ to represent an unlabelled 2D pose from the target dataset. Given the intrinsic parameters \mathbf{K} of the camera from the target dataset, our method synthesizes augmented and aligned 2D and 3D pose pairs $\mathbf{P}' = (\mathbf{P}'_{2D}, \mathbf{P}'_{3D})$ with

$$\begin{aligned} \mathbf{P}'_{3D} &= G(\mathbf{P}_{2D}^{src}, \mathbf{P}_{3D}^{src}, \mathbf{P}_{2D}^{tgt}), \\ \mathbf{P}'_{2D} &= F(\mathbf{P}'_{3D}, \mathbf{K}), \end{aligned} \quad (1)$$

where G denotes a generator function and F is the projection function from 3D camera coordinates to 2D image coordinates.

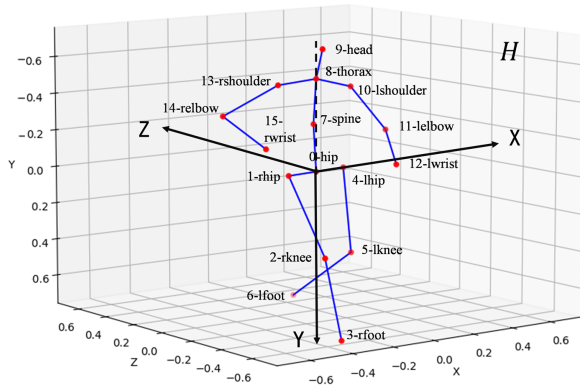


Fig. 3. **Human skeleton joints and human-centric coordinate system.** Where relevant, each joint’s label is preceded with ‘r’ and ‘l’ for right and left sides.

The synthesized pose pairs are used to fine-tune the Pose Estimator M_e with parameters ϕ_e by minimizing

$$\min_{\phi_e} L_e(M_e(\mathbf{P}'_{2D}, \phi_e), \mathbf{P}'_{3D}), \quad (2)$$

where L_e denotes the loss function between predicted and ground truth 3D poses.

B. Overview of the Proposed Method

Our proposed framework aims to synthesize new 2D-3D pose pairs from the labeled source domain and the unlabeled target domain, and then use them to train a pose estimator to predict the 3D human pose in the target domain. Among the various factors contributing to the domain gap, camera viewpoints and positions play a significant role by affecting the global positions of the poses. Thus, the key challenge to be met is how to make the augmented data adequately match the distribution of the target dataset. To achieve this, we explore the latent knowledge of the target dataset as follows (also illustrated in Fig. 2). A Pseudo-Label Generation module M_p for the *target dataset* is proposed to generate pseudo-3D poses. For the *source dataset*, we employ an augmentation module, Pose Augmentor M_a , that creates more diverse samples to better account for motions and body sizes. The 2D and 3D poses from both domains are then spatially aligned in a Global Transformation module M_t using a human-centric coordinate system as a bridge. These aligned 2D-3D pairs are then fed into a Pose Discriminator M_d to distinguish reliable poses to be used to fine-tune the Pose Estimator M_e . Finally, the Pose Estimator M_e is applied to the target dataset to generate updated 3D pseudo-labels. Since the Global Transformation module is guided by pseudo-labels, updated pseudo-labels enhance alignment between synthesized and target data. Therefore, it may be possible to boost the pose estimation results by iterating the above process. We explore this in our ablations.

C. Pseudo-Label Generation

For the target dataset, we generate 3D pseudo-labels by inferring absolute 3D coordinates of human skeleton joints

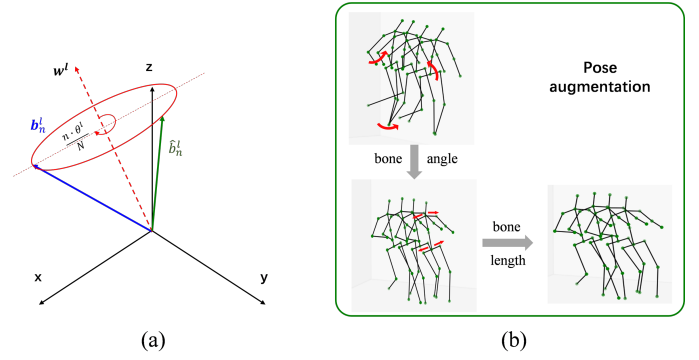


Fig. 4. (a) **Bone angle augmentation for a 3D pose sequence.** (b) **A source 3D pose sequence is augmented by modifying its motion via bone angle operation and body size via bone length operation.**

in the camera coordinate system from the available 2D labels. These 3D pseudo-labels can be obtained using a pre-trained pose estimation method given 2D inputs.

Given a 2D pose $\mathbf{P}_{2D}^{tgt} = [\mathbf{x}^{tgt}, \mathbf{y}^{tgt}]^T$ from the target dataset, we obtain the root-relative 3D coordinates $\hat{\mathbf{P}}_{3D}^{tgt} = [\hat{\mathbf{X}}^{tgt}, \hat{\mathbf{Y}}^{tgt}, \hat{\mathbf{Z}}^{tgt}]^T$ using VideoPose3D [23], pretrained on the source dataset¹. The predicted 3D coordinates of the joints $(\hat{X}_j^{tgt}, \hat{Y}_j^{tgt}, \hat{Z}_j^{tgt}), j = \{0, \dots, J-1\}$ are root-relative 3D coordinates with the root $(\hat{X}_0^{tgt}, \hat{Y}_0^{tgt}, \hat{Z}_0^{tgt})$ set to $(0, 0, 0)$. To obtain the absolute coordinates of the root, we apply a two-stage optimization process. In the first stage, given the 2D pose and camera intrinsic parameters \mathbf{K} , the 3D pose can be inferred by assuming an initial depth value.

The corresponding bone lengths are then derived from the estimated 3D pose. To ensure anatomical consistency, we minimize the discrepancy between the estimated bone lengths and their averaged values using least squares, and thus, we obtain the 3D absolute coordinates of all joints $\tilde{\mathbf{P}}_j = (\tilde{X}_j^{tgt}, \tilde{Y}_j^{tgt}, \tilde{Z}_j^{tgt}), j = \{0, \dots, J-1\}$. In the second stage, we minimize the error between reprojected 2D pose from $\tilde{\mathbf{P}}_{3D}^{tgt} + \mathbf{P}_r$ and real 2D pose \mathbf{P}_{2D}^{tgt} , where \mathbf{P}_r is the absolute coordinates of the root joint and its initial value is set to root joint $\tilde{\mathbf{P}}_0$. Finally, we arrive at the estimated absolute 3D coordinates of all joints $\tilde{\mathbf{P}}_{3D}^{tgt}$ as the 3D pseudo-labels of the target dataset.

D. Pose Augmentor

The poses in the source dataset are augmented using the bone augmentation process from AdaptPose [18]. This allows our Pose Augmentor M_a to modify bone angles across frames to introduce greater diversity in motion representation and ensure the augmented poses capture a wider range of actions. Additionally, bone lengths are adjusted to accommodate variations in human body proportions, enhancing the model’s adaptability to different body sizes.

Given a sequence of 3D poses $\{\mathbf{P}_{3D}^{src}\}_{n=0}^{N-1}$ from the source dataset, our augmentor converts them into their corresponding bone vectors $\{\mathbf{B}^{src}\}_{n=0}^{N-1} \in R^{N \times (J-1) \times 3}$. Each original bone vector $b_n^l \in R^{1 \times 3}$ (i.e., the l -th bone vector from \mathbf{B}^{src}

¹We tried other methods, e.g. MixSTE [24], obtaining very similar results.

in n -th frame) is rotated about an axis $\mathbf{w} \in R^{(J-1) \times 3}$ by a certain rotation angle $\theta \in R^{(J-1) \times 3}$ proportional to the number of frames. This guarantees that the bone changes are temporally plausible and consistent. Additionally, to adjust the bone length, the pose augmentor scales it using a ratio parameter $\lambda \in R^{(J-1) \times 3}$, which systematically modifies the bone length while preserving the structural coherence of the motion.

To predict the parameters $(\mathbf{w}, \theta, \lambda)$, a Gaussian-noise vector is concatenated with the input 3D pose of the middle frame to introduce randomness and diversity for feature extraction. Subsequently, four fully connected layers followed by batch normalization and a leaky ReLU are used to extract features and learn these parameters [18].

An example of the above process is shown in Fig. 4(a), where by rotating \mathbf{b}_n^l along the axis \mathbf{w}^l for $\frac{n \cdot \theta^l}{N}$ degrees, we obtain the augmented bone vectors $\hat{\mathbf{b}}_n^l$ with revised joint angles. Then, we apply the bone length ratio λ^l to obtain $(1 + \lambda^l) \cdot \hat{\mathbf{b}}_n^l$ as the new bone vector. All the new bone vectors $\hat{\mathbf{B}} \in R^{N \times (j-1) \times 3}$, where $(1 + \lambda^l) \cdot \hat{\mathbf{b}}_n^l$ is the l -th bone vector of n -th frame, are then converted back to generate the augmented 3D pose sequence $\{\mathbf{P}_{3D}^A\}_{n=0}^{N-1}$. Fig. 4(b) illustrates examples of the effects of the bone angle and bone length augmentation.

E. Global Transformation

The Global Transformation module M_t is designed to eliminate differences in camera viewpoints and positions between the source and target domains. To achieve the optimal alignment of 3D coordinates from both domains, we propose a human-centric coordinate system as a bridge. As shown in Fig. 3, the origin of this coordinate system H is centered at the middle of the left and right hip joints. The x -axis is defined as the unit vector pointing from the origin to the right hip, while the x - y plane is defined by three joints: the left hip, right hip, and thorax joint. The z -axis is determined by the unit vector perpendicular to x - y plane and y -axis is the cross-product of x and z axes.

Given an augmented 3D pose \mathbf{P}_{3D}^A from the source dataset under the source camera coordinate system C_s , we transform it using rotation and translation matrices $(\mathbf{R}_1, \mathbf{T}_1)$ from C_s to H , where H is our human coordinate system (see Fig. 3). Similarly, given a 3D pseudo-pose $\tilde{\mathbf{P}}_{3D}^{tgt}$ sampled from the target dataset (that were generated earlier in Section III-C) under the target camera coordinate system C_t , we compute the corresponding rotation and translation matrices $(\mathbf{R}_2, \mathbf{T}_2)$ from C_t to H . The transformation from any camera coordinate system to the human-centric coordinate system H is outlined in Algorithm 1 (See Appendix).

Using the human coordinate system H as a bridge, the discrepancy between the source and target domains in terms of positions can be determined from variations of the subject's position and orientation relative to the camera. Thus, to eliminate this discrepancy, we first obtain

$$\mathbf{P}_H = \mathbf{R}_1 \cdot (\mathbf{P}_{3D}^A + \mathbf{T}_1), \quad (3)$$

where \mathbf{P}_H denotes the 3D human pose in the human centered coordinate system. Then, we convert \mathbf{P}_H into the target camera

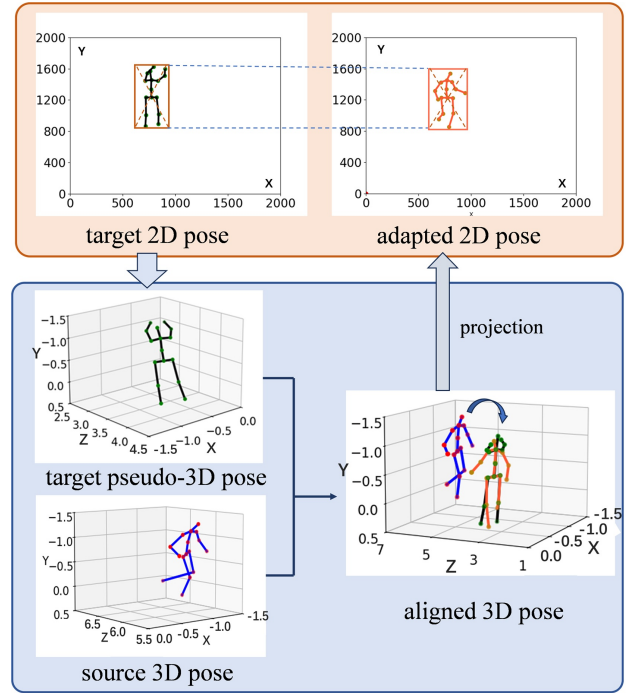


Fig. 5. **Visualization of the global transformation.** The target pseudo-3D pose inferred from the target 2D pose guides rotation and translation of the source 3d pose to generate the aligned 3D pose. Given the aligned 3D poses, corresponding 2D poses are obtained through projection using the intrinsic camera parameters of the target dataset so that the 2D root positions are also aligned.

coordinate system C_t to enable the synthesis of new data from \mathbf{P}_{3D}^A , such that

$$\mathbf{P}'_{3D} = \mathbf{R}_2^{-1} \cdot \mathbf{P}_H - \mathbf{T}_2, \quad (4)$$

where $\mathbf{P}'_{3D} = [\mathbf{X}', \mathbf{Y}', \mathbf{Z}']^T \in R^{3 \times J}$, ensuring alignment with the target domain. Finally, we can project \mathbf{P}'_{3D} into 2D pose $\mathbf{P}'_{2D} = [\mathbf{u}, \mathbf{v}]^T \in R^{2 \times J}$ where (\mathbf{u}, \mathbf{v}) denote the 2D image coordinates, obtained as

$$\begin{aligned} u_j &= f_x \cdot \frac{X'_j}{Z'_j} + c_x, \\ v_j &= f_y \cdot \frac{Y'_j}{Z'_j} + c_y, \quad j = \{0, \dots, J-1\} \end{aligned} \quad (5)$$

where (f_x, f_y, c_x, c_y) are the target dataset camera's intrinsic parameters. As shown in Fig. 5, after global transformation, 3D poses from the source and target domains are optimally aligned. For 2D poses, their root positions are also aligned and the scales are similar. This alignment process significantly reduces the domain discrepancies caused by differences in camera viewpoints and positions.

F. Iterative training architecture

After obtaining the aligned 2D and 3D poses \mathbf{P}'_{2D} and \mathbf{P}'_{3D} respectively, we train an adversarial pose augmentation framework to ensure the fidelity of the generated human poses (following previous works [17], [21]). This augmentation framework involves our generator, i.e., the pose augmentor M_a and the discriminator M_d . The discriminator performs two

tasks. First, it uses the aligned 2D pose \mathbf{P}'_{2D} and the target 2D pose \mathbf{P}^{tgt}_{2D} at the middle frame as input, to adjust \mathbf{P}'_{2D} to closely match the target sample. This is unlike PoseAug [17] which uses the 2D poses of source dataset as input. In the second task, the discriminator uses the middle-frame 3D augmented pose \mathbf{P}^A_{3D} and the source pose \mathbf{P}^{src}_{3D} as input to ensure the fidelity of poses after bone angle and bone length augmentation. Inspired by Kinematic Chain Space (KCS) [49], [50], we use KCS representation of 3D pose as input rather than 3D joints.

In each epoch, the generator M_a , discriminator M_d and the pose estimator M_e are trained jointly. Their loss functions are as follows.

Discriminator loss. We use least squares GAN (LSGAN) [51] to train the adversarial pose augmentation framework:

$$\begin{aligned} L_{dis} &= L_{dis}^{2D} + L_{dis}^{3D}, \\ L_{dis}^{2D} &= \frac{1}{2}\mathbb{E}[M_d^{2D}(\mathbf{P}'_{2D}) - 1]^2 + \frac{1}{2}\mathbb{E}[M_d^{2D}(\mathbf{P}^{tgt}_{2D})^2], \\ L_{dis}^{3D} &= \frac{1}{2}\mathbb{E}[(M_d^{3D}(\mathbf{P}^{src}_{3D}) - 1)^2] + \frac{1}{2}\mathbb{E}[M_d^{3D}(\mathbf{P}^A_{3D})^2]. \end{aligned} \quad (6)$$

Generator loss. The adversarial loss of the generator M_a is the feedback from the discriminator:

$$\begin{aligned} L_{adv} &= \alpha \cdot L_{adv}^{2D} + \beta \cdot L_{adv}^{3D}, \\ L_{adv}^{2D} &= \frac{1}{2}\mathbb{E}[(M_d^{2D}(\mathbf{P}'_{2D}) - 1)^2] + \frac{1}{2}\mathbb{E}[M_d^{2D}(\mathbf{P}^{tgt}_{2D})^2], \\ L_{adv}^{3D} &= \frac{1}{2}\mathbb{E}[(M_d^{3D}(\mathbf{P}^A_{3D}) - 1)^2] + \frac{1}{2}\mathbb{E}[M_d^{3D}(\mathbf{P}^{src}_{3D})^2]. \end{aligned} \quad (7)$$

Pose estimation loss. The standard Mean Squared Error (MSE) loss is employed for the Pose Estimator M_e ,

$$L_S = \left\| \mathbf{P} - \tilde{\mathbf{P}} \right\|_2^2, \quad (8)$$

where \mathbf{P} and $\tilde{\mathbf{P}}$ are the ground truth and predicted 3D poses respectively. Before training M_e , the generator and the discriminator need to be warmed up for m epoch.

After the training process, we obtain a fine-tuned Pose Estimator M_e which generates predicted 3D poses $\hat{\mathbf{P}}^{tgt}_{3D}$ for the target dataset. These poses could be used as input for the Pseudo-Label Generation module M_p again, and thus, the training process can be iterative and the number of iterations are studied in the ablation study.

IV. EXPERIMENTS

A. Datasets and Metrics

Following previous works, we evaluate our method on several widely used large-scale 3D human pose estimation benchmarks, including MPI-INF-3DHP [43], 3DPW [52] and Human3.6M [53].

MPI-INF-3DHP (3DHP) is a large-scale, in-the-wild 3D human pose dataset. It includes 2D and 3D data from eight subjects performing eight different activities, recorded in both indoor and outdoor scenes. 3DHP is ideal for evaluating methods that aim to generalize to real-world scenarios. We follow previous works [17], [54] by using the test set, which consists of approximately 2,929 frames. Evaluation is conducted using three main metrics: Mean Per Joint Position Error (MPJPE), Percentage of Correct Keypoints (PCK) with a 150mm threshold, and Area Under the Curve (AUC) calculated over various PCK thresholds.

3D Poses in the Wild Dataset (3DPW) offers a unique and challenging benchmark for 3D human pose estimation in a variety of uncontrolled outdoor settings. It includes dynamic camera motion and natural lighting conditions, with scenes recorded at 25 fps. In evaluations, MPJPE and Procrustes-Aligned Mean Per Joint Position Error (PA-MPJPE) are used as evaluation metrics.

Human3.6M (H3.6M) is an extensive dataset for 3D human pose estimation, captured in a controlled indoor environment. The dataset includes over 3.6m frames, covering seven main subjects (S1, S5, S6, S7, S8, S9, and S11) engaged in 15 diverse activities. Following previous works [20], [21], H3.6M has two main settings: (i) for cross-dataset evaluation, we use subjects S1, S5, S6, S7, and S8 as the source domain, with the other dataset as the target domain, and (ii) for cross-scenario evaluation, we use only S1 as the source domain, with S5, S6, S7, and S8 as the target domain. Measures MPJPE and PA-MPJPE are standard metrics employed to evaluate performance across these tasks.

B. Implementation Details

Pose Estimator. Following previous works [17], [18], [22], we use single-frame-based VideoPose3D [23] and video-based MixSTE [24] for our Pose Estimator M_e . The input sequence lengths of MixSTE was set to 27 for 3DHP and 3DPW, and 243 for Human3.6M following the settings in [22]. The pre-trained weights from the source dataset are used as initial weights. We adopt the 16-keypoint human model with 0-th joint (hip center point) as the origin and we use ground truth 2D keypoints as input.

Generators and discriminators. The generator M_a has three 3-layer residual MLPs with LeakyReLU to generate augmented bone angles and bone lengths. We set $\alpha = 1$ and $\beta = 6$ in Eq. 7. The Pose Discriminator M_d uses the same architecture for processing both 2D and 3D poses, consisting of five 4-layer residual MLPs with LeakyReLU with each corresponding to a part of KCS representation.

Training. The initial learning rates for the discriminator, generator, and pose estimator are all set to 0.0001. They all use Adam optimizer. The experiments are conducted with a batch size of 1024 for 50 epochs and there is a warm-up phase lasting 2 epochs to train the generator and discriminator.

C. Results

Cross-dataset Evaluation. For cross-dataset evaluations, the source and target data exhibit large domain gaps in terms of camera settings, human body size, and motions. We perform three cross-dataset experiments.

In the first, H3.6M is the source and 3DHP is the target dataset (see Table I). For single frame-based VideoPose3D [23] as the Pose Estimator M_e , our method outperforms PoSynDA [22] by 2.5mm↓ on MPJPE and PoseDA [21] by 2.1↑ on AUC. For video-based MixSTE [24] as the Pose Estimator, our method improves on PoSynDA [22] by 4.2mm↓ in MPJPE, 0.9%↑ in PCK and 5.4↑ in AUC. Note, our method using MixSTE [24] surpasses the target-specific, fully supervised

TABLE I

Cross-dataset evaluation results on target 3DHP with source H3.6M.
 FIRST TWO METHODS MARKED WITH * WERE FULLY-SUPERVISED, I.E.,
 TRAINED AND TESTED ON 3DHP. ‘Vid’ DENOTES METHOD IS
 VIDEO-BASED WITH $T = 27$. VIDEOPOSE3D [23] (VP3D) AND MIXSTE
 [24] ARE INDICATED AS THE POSE ESTIMATOR USED IN EACH METHOD.

Method		Vid	MPJPE ↓	PCK ↑	AUC ↑
SimpleBaseline [36] *	ICCV2017		84.3	85.0	52.0
MixSTE [24] *	CVPR2022		54.9	94.4	66.5
PoseAug (VP3D) [17]	CVPR2021		73.0	88.6	57.3
PoseDA (VP3D) [21]	ICCV2023		61.3	92.1	62.5
PoSynDA (VP3D) [22]	ACMMM2023		60.2	93.1	58.4
Dual-Augmentor (VP3D) [20]	CVPR2024		63.1	92.9	60.7
Ours (VP3D)			57.7	92.5	64.6
AdaptPose (VP3D) [18]	CVPR2022	✓	68.3	90.2	59.0
PoSynDA (MixSTE) [22]	ACMMM2023	✓	58.2	93.5	59.6
Ours (MixSTE)		✓	54.0	94.4	65.0

TABLE II

Cross-dataset evaluation results on target 3DPW with source H3.6M.
 FIRST TWO METHODS MARKED WITH * WERE FULLY-SUPERVISED, I.E.,
 TRAINED AND TESTED ON 3DPW. ‘Vid’ DENOTES METHOD IS
 VIDEO-BASED WITH $T = 27$. VIDEOPOSE3D [23] (VP3D) AND MIXSTE
 [24] ARE INDICATED AS THE POSE ESTIMATOR USED IN EACH METHOD.

Method		Vid	MPJPE ↓	PA-MPJPE ↓
VIBE [55] *	CVPR2020	✓	82.9	51.9
Lin et al. [56] *	ICCV2021		74.7	45.6
PoseAug (VP3D) [17]	CVPR2021		94.1	58.5
PoseDA (VP3D) [21]	ICCV2023		87.7	55.3
Dual-Augmentor (VP3D) [20]	CVPR2024		106.6	73.2
Ours (VP3D)			75.7	45.1
VIBE [55]	CVPR2020	✓	93.5	56.5
BOA [48]	CVPR2021	✓	77.2	49.5
AdaptPose (VP3D) [18]	CVPR2022	✓	81.2	46.5
PoSynDA (MixSTE) [22]	ACMMM2023	✓	75.5	45.4
Ours (MixSTE)		✓	66.6	41.9

MixSTE [24] method itself (from 54.9mm to 54.0mm in MPJPE).

In the second experiment, H3.6M is the source and 3DPW is the target dataset (see Table II). For both single-frame and video-based methods, our approach achieve state-of-the-art results. Amongst single-frame methods, ours surpasses PoseDA [21] in MPJPE by 12.0mm↓ and in PA-MPJPE by 10.2mm↓ respectively. For video-based approaches, again in comparison with the state-of-the-art PoSynDA [22], we improve by 8.9mm↓ and 3.5mm↓ in MPJPE and PA-MPJPE, respectively. Our method manages greater strides in improved results on 3DPW than on 3DHP, as it is designed to address the issue of variations in camera position and orientation which are more pertinent to the dynamic camera motion scenes in 3DPW.

In the third experiment, we demonstrate the effectiveness of our method given a challenging viewpoint. We add to the 3DHP dataset a simulated virtual camera C_v , positioned at 2m above the ground plane at a depression angle of 45° . For ease of exposition, we call this dataset, 3DHP-C. We compute new 3D poses under the coordinate system of the virtual camera and then use the intrinsic parameters of the original camera in 3DHP dataset to compute 2D poses, such that

$$\begin{bmatrix} X_{new} \\ Y_{new} \\ Z_{new} \end{bmatrix} = \begin{bmatrix} 1 & 0 & 0 \\ 0 & \cos(45^\circ) & \sin(45^\circ) \\ 0 & \sin(45^\circ) & \cos(45^\circ) \end{bmatrix} \cdot \begin{bmatrix} X \\ Y + 2 \\ Z \end{bmatrix}, \quad (9)$$

$$\begin{bmatrix} u_{new} \\ v_{new} \\ 1 \end{bmatrix} = \begin{bmatrix} f_x^p & 0 & c_x^p \\ 0 & f_y^p & c_y^p \\ 0 & 0 & 1 \end{bmatrix} \cdot \begin{bmatrix} \frac{X_{new}}{Z_{new}} \\ \frac{Y_{new}}{Z_{new}} \\ 1 \end{bmatrix},$$

where (X, Y, Z) is the 3D coordinate of a joint in 3DHP, $(X_{new}, Y_{new}, Z_{new})$ is the 3D coordinate of the joint in 3DHP-C after processing, $((f_x^p, f_y^p, c_x^p, c_y^p))$ are the intrinsic parameters of the original camera in 3DHP, and (u_{new}, v_{new}) is the 2D coordinate of the joint in 3DHP-C.

Table III presents comparative results against PoseAug [17] and AdaptPose [18] with H3.6M as source and 3DHP-C as the target dataset. We do not compare with PoseDA [21] as their complete codes are not available, nor with PoSynDA [22] since we obtained excessively incorrect results using their provided code. Our method outperforms by a large margin. This improvement stems from our explicit handling of camera viewpoint discrepancies which impresses the potential effectiveness of the proposed method under challenging viewpoints.

Cross-scenario Evaluation. In cross-scenario evaluations, subject S1’s data in H3.6M is the source and subjects S5, S6, S7, and S8’s data in H3.6M are the target. As shown in Table IV, among related work, our method performs slightly better in MPJPE, and (almost) as well in PA-MPJPE. In this experiment, the camera parameters do not change much between subjects.

TABLE III

Cross-dataset evaluation results on target 3DHP-C with source H3.6M.
 VIDEOPOSE3D [23] (VP3D) AND MIXSTE [24] ARE INDICATED AS THE
 POSE ESTIMATOR USED IN EACH METHOD.

Method		MPJPE ↓	PCK ↑	AUC ↑
PoseAug (VP3D) [17]	CVPR2021	145.4	61.2	33.3
AdaptPose (VP3D) [18]	CVPR2022	132.8	65.0	35.6
Ours (VP3D)		77.3	87.6	54.5
Ours (MixSTE)		57.8	92.0	64.1

TABLE IV

Cross-scenario evaluation results on target H3.6M (S5,S6,S7,S8) with source H3.6M (S1). ‘Vid’ DENOTES METHOD IS VIDEO-BASED WITH $T = 243$. VIDEOPOSE3D [23] (VP3D) AND MIXSTE [24] ARE INDICATED AS THE POSE ESTIMATOR USED IN EACH METHOD.

Method		Vid	MPJPE ↓	PA-MPJPE ↓
VideoPose3D [23]	CVPR2019		64.7	-
Li et al. [34]	CVPR2020		62.9	-
PoseAug (VP3D) [17]	CVPR2021		56.7	-
PoseDA (VP3D) [21]	ICCV2023		49.9	34.2
Dual-Augmentor (VP3D) [20]	CVPR2024		50.3	-
Ours (VP3D)			49.7	34.2
AdaptPose (VP3D) [18]	CVPR2022	✓	54.2	35.6
PoSynDA (MixSTE) [22]	ACMMM2023	✓	48.1	33.2
Ours (MixSTE)		✓	47.9	33.5

Qualitative evaluation. Fig. 6 (a)-(d) presents example qualitative results on the 3DHP dataset which show that compared to the pre-trained baseline model VideoPose3D [23], our method performs significantly better, especially for joints that are farther away from the root joint. Fig. 6(e) illustrates a failure case of our method where the estimation of joints

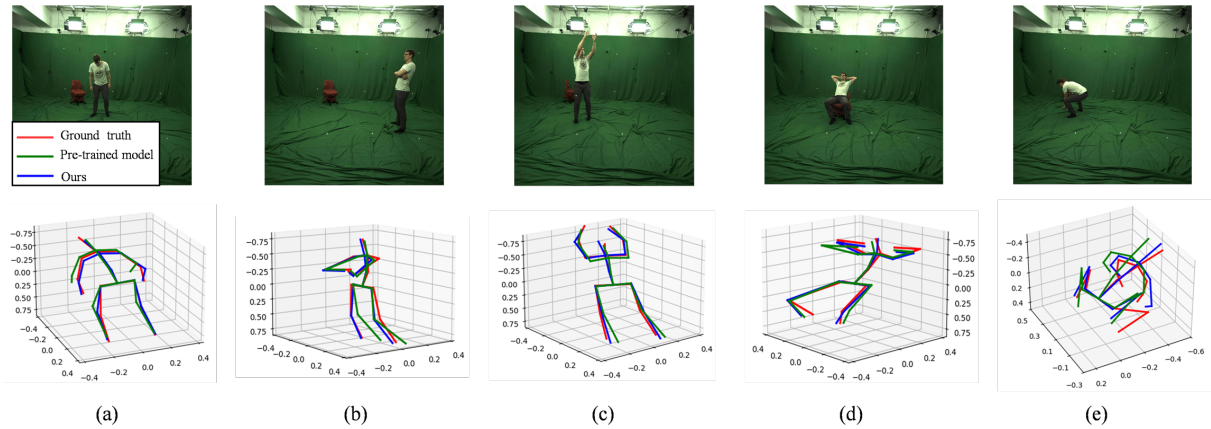


Fig. 6. **Example 3D pose estimations on 3DHP dataset.** (a)-(d) Our method (blue) performs significantly better than the pre-trained model (green) within smaller error compared with the ground truth (red). (e) In cases of severe self-occlusion, our method fails to obtain sufficiently estimations.

on the right side of the body is not accurate enough due to extreme self-occlusion.

D. Ablation Study

We conduct a series of ablation studies with H3.6M as the source domain and 3DHP as the target domain. We employ the ground truth 2D poses as input and VideoPose3D [23] as the Pose Estimator.

Effect of method’s modules. We conduct an ablation study starting from a baseline model that was trained on the source domain, with our method’s modules systematically integrated to analyze their effects: Pose Augmentor M_a , Pseudo-Label Generation module M_p , Global Transformation module M_t , and iterative training.

As shown in Table V, when our Pose Augmentor M_a is added we achieve an improvement of 6.1mm \downarrow in MPJPE, followed by a substantial error reduction of 20.6mm \downarrow when the Global Transformation module M_t with pseudo-labels from M_p are introduced. Finally, through an iteration of the whole process, a further drop of 0.8mm \downarrow in MPJPE is achieved. Corresponding increases in PCK and AUC are also shown.

TABLE V
The impact of each module in proposed method. THE * INDICATES THAT THE MODULES WERE PROCESSED FOR AN EXTRA ITERATION.

Method	MPJPE \downarrow	PCK \uparrow	AUC \uparrow
VideoPose3D [23]	85.3	84.1	52.9
VideoPose3D [23] + M_a	79.2	86.5	54.9
VideoPose3D [23] + M_a + (M_p & M_t)	58.6	91.8	64.3
VideoPose3D [23] + M_a + (M_p & M_t)*	57.7	92.5	64.6

Different Global Transformations. The global transformation module M_t contributes significantly in reducing the domain differences in camera positions and orientations from source to target. It is target-oriented and uses the pseudo-labels to guide the rotation and translation of the 3D poses. We compare three other approaches to a global transformation: RR+RT, GR+RT, RR+GT, where RR denotes rotation matrices are randomly initialized and learned in the network, RT denotes the translation matrices are randomly initialized and

learned in the network, GR denotes the pseudo-label guided rotation and GT denotes the pseudo-label guided translation. Our approach is therefore GR+GT, which performs best as shown in Table VI.

TABLE VI
The impact of different approaches to Global Transformation M_t .

Global Transformation	MPJPE \downarrow	PCK \uparrow	AUC \uparrow
RR+RT	73.0	88.6	57.3
GR+RT	66.0	89.9	60.9
RR+GT	63.7	90.3	62.0
GR+GT	57.7	92.5	64.6

Number of iterations. The influence of the number of iterations on the model’s performance is shown in Table VII. The results are averaged after five runs with different random seed values. Beyond one round of iteration, the model fails to gain further increments and a possible reason could be overfitting.

TABLE VII
The impact of using different number of iterations.

Iterations	MPJPE \downarrow	PCK \uparrow	AUC \uparrow
0	58.6	91.8	64.3
1	57.7	92.5	64.6
2	58.2	92.0	64.3
3	58.0	92.3	64.4
4	58.3	92.0	64.3

Different hyperparameters of the loss function. The impact of different hyperparameter settings in the Generator loss function is tested and reported in Table VIII. Based on our empirical investigation, we set $\alpha = 1$, $\beta = 6$ in the model.

E. Discussion Compared to SOTA Methods

The most recent state-of-the-art works in the field of unsupervised domain adaptation for 3D human pose estimation include PoseDA [21], PoSynDA [22], and the Dual-Augmentor framework [20]. Our method presents notable differences and advantages over them.

TABLE VIII
 The impact of different hyperparameters in Generator loss function.

α	β	MPJPE↓	PCK↑	AUC↑
1	1/3	63.5	90.6	62.6
1	1	62.4	91.0	62.7
1	3	59.7	91.7	63.2
1	6	57.7	92.5	64.6
1	9	58.2	92.3	64.4
1	18	58.8	92.1	64.1

PoseDA [21] aligns global positions of 3D poses to ensure their projected 2D poses match the target dataset in scale and position. While this aligns 2D poses across domains, it does not fully address the inherent ambiguity in mapping 2D to 3D. Our method aligns both 2D and 3D poses, ensuring a closer match between source and target domains in both input and label spaces. PoSynDA [22] builds on PoseDA by leveraging a diffusion-based model (D3DP [40]) to generate multiple pseudo-labels for the target domain. However, using a diffusion model increases model complexity, whereas, our approach introduces no additional training parameters in the Global Transformation module M_t .

The Dual-Augmentor framework [20] generates diverse out-of-source distributions using a weak and strong augmentor, but it does not exploit 2D poses from the target domain, limiting its performance in cross-dataset evaluation. Our method fully utilizes target-domain 2D poses to generate pseudo-3D poses, guiding global transformations that better align 3D across domains. Additionally, our Pose Discriminator incorporates 2D poses from the target domain, ensuring that generated 2D poses also align with the target distribution.

V. CONCLUSION

This paper proposes an iterative framework for domain-adaptive human pose estimation, focusing on aligning the 2D and 3D poses across domains to bridge domain gaps. A Pseudo-Label guided Global Transformation module incorporates a human-centered coordinate system to explicitly align the global coordinates between source and target domains. This design is both intuitive and effective, achieving significant performance gains without adding extra training parameters. Additionally, we enhance pose augmentation by modifying bone lengths and angles, and we propose to use an adversarial learning architecture based on the target domain’s 2D poses and the source domain’s 3D poses.

Extensive experiments on three public datasets demonstrate that our approach can surpass or compete with state-of-the-art models and outperform the target-domain trained model MixSTE [24]. This included experiments where we added a simulated, challenging camera viewpoint to the 3DHP dataset to validate our method’s robustness in even more difficult scenarios. For future work, we shall explore source-free domain adaptive human pose estimation without requiring access to source data.

ACKNOWLEDGMENTS

This work was supported by the TORUS Project, which has been funded by the UK Engineering and Physical Sciences

Research Council (EPSRC), grant number EP/X036146/1.

APPENDIX

Algorithm 1 Computation of the transformation matrices \mathbf{R}, \mathbf{T} from camera coordinate system C to human-centric coordinate system H .

Input: coordinates of 3D pose $\mathbf{P}_j = (X_j, Y_j, Z_j), (j = 0, \dots, J - 1)$ under C , where j denotes the j -th joint.

Output: rotation matrix \mathbf{R} and translation matrix \mathbf{T}

// Computation of the unit vector along x-axis, which is pointing from the left hip (4th joint) to the right hip (1st joint)

$$\mathbf{v}_{1_4} = \mathbf{P}_1 - \mathbf{P}_4$$

$$\mathbf{e}_1 = \mathbf{v}_{1_4} / \|\mathbf{v}_{1_4}\|$$

// Computation of the unit vector along z-axis, which is perpendicular to the plane comprising the right hip (1st joint), left hip (4th joint) and thorax (8th joint)

$$\mathbf{v}_{0_8} = \mathbf{P}_8 - (\mathbf{P}_1 + \mathbf{P}_4) / 2$$

$$\mathbf{k}_t = \mathbf{e}_1 \times \mathbf{v}_{0_8}$$

$$\mathbf{e}_3 = \mathbf{k}_t / \|\mathbf{k}_t\|$$

// Computation of the unit vector along y-axis, which is perpendicular to the x and z axes

$$\mathbf{e}_2 = \mathbf{e}_1 \times \mathbf{e}_3$$

$$\tilde{\mathbf{R}} = [\mathbf{e}_1; \mathbf{e}_2; \mathbf{e}_3]$$

$$\tilde{\mathbf{T}} = (\mathbf{P}_1 + \mathbf{P}_4) / 2$$

$$\mathbf{R} = \tilde{\mathbf{R}}^{-1}$$

$$\mathbf{T} = -\tilde{\mathbf{T}}$$

REFERENCES

- [1] Y. Jiao, H. Yao, and C. Xu, “Pen: Pose-embedding network for pedestrian detection,” *IEEE Transactions on Circuits and Systems for Video Technology*, vol. 31, no. 3, pp. 1150–1162, 2020.
- [2] L. Wu, C. Huang, L. Fei, S. Zhao, J. Zhao, Z. Cui, and Y. Xu, “Video-based fall detection using human pose and constrained generative adversarial network,” *IEEE Transactions on Circuits and Systems for Video Technology*, 2023.
- [3] V. Guzov, A. Mir, T. Sattler, and G. Pons-Moll, “Human positioning system (hps): 3d human pose estimation and self-localization in large scenes from body-mounted sensors,” in *Proceedings of the IEEE/CVF Conference on Computer Vision and Pattern Recognition*, 2021, pp. 4318–4329.
- [4] H. Yi, C.-H. P. Huang, S. Tripathi, L. Hering, J. Thies, and M. J. Black, “Mime: Human-aware 3d scene generation,” in *Proceedings of the IEEE/CVF Conference on Computer Vision and Pattern Recognition*, 2023, pp. 12965–12976.
- [5] N. Haouchine, P. Juvekar, M. Nercessian, W. M. Wells III, A. Golby, and S. Frisken, “Pose estimation and non-rigid registration for augmented reality during neurosurgery,” *IEEE Transactions on Biomedical Engineering*, vol. 69, no. 4, pp. 1310–1317, 2021.
- [6] H. Yu, X. Fan, Y. Hou, W. Pei, H. Ge, X. Yang, D. Zhou, Q. Zhang, and M. Zhang, “Toward realistic 3d human motion prediction with a spatio-temporal cross-transformer approach,” *IEEE Transactions on Circuits and Systems for Video Technology*, vol. 33, no. 10, pp. 5707–5720, 2023.
- [7] Z. Lu, H. Wang, Z. Chang, G. Yang, and H. P. Shum, “Hard no-box adversarial attack on skeleton-based human action recognition with skeleton-motion-informed gradient,” in *Proceedings of the IEEE/CVF International Conference on Computer Vision*, 2023, pp. 4597–4606.
- [8] C. Zimmermann, T. Welschhold, C. Dornhege, W. Burgard, and T. Brox, “3d human pose estimation in rgb-d images for robotic task learning,” in *2018 IEEE International Conference on Robotics and Automation (ICRA)*. IEEE, 2018, pp. 1986–1992.
- [9] H. Liu and L. Wang, “Collision-free human-robot collaboration based on context awareness,” *Robotics and Computer-Integrated Manufacturing*, vol. 67, p. 101997, 2021.

- [10] M. Svenstrup, S. Tranberg, H. J. Andersen, and T. Bak, "Pose estimation and adaptive robot behaviour for human-robot interaction," in *2009 IEEE International Conference on Robotics and Automation*. IEEE, 2009, pp. 3571–3576.
- [11] R. Huo, Q. Gao, J. Qi, and Z. Ju, "3d human pose estimation in video for human-computer/robot interaction," in *International Conference on Intelligent Robotics and Applications*. Springer, 2023, pp. 176–187.
- [12] R. Gu, G. Wang, Z. Jiang, and J.-N. Hwang, "Multi-person hierarchical 3d pose estimation in natural videos," *IEEE Transactions on Circuits and Systems for Video Technology*, vol. 30, no. 11, pp. 4245–4257, 2019.
- [13] B. Wandt, M. Rudolph, P. Zell, H. Rhodin, and B. Rosenhahn, "Canon-pose: Self-supervised monocular 3d human pose estimation in the wild," in *Proceedings of the IEEE/CVF conference on computer vision and pattern recognition*, 2021, pp. 13 294–13 304.
- [14] Z. Tang, Y. Hao, J. Li, and R. Hong, "Ftcm: Frequency-temporal collaborative module for efficient 3d human pose estimation in video," *IEEE Transactions on Circuits and Systems for Video Technology*, vol. 34, no. 2, pp. 911–923, 2023.
- [15] L. Zhou, Y. Chen, and J. Wang, "Dual-path transformer for 3d human pose estimation," *IEEE Transactions on Circuits and Systems for Video Technology*, 2023.
- [16] J. Zhang, X. Nie, and J. Feng, "Inference stage optimization for cross-scenario 3d human pose estimation," *Advances in neural information processing systems*, vol. 33, pp. 2408–2419, 2020.
- [17] K. Gong, J. Zhang, and J. Feng, "Poseaug: A differentiable pose augmentation framework for 3d human pose estimation," in *Proceedings of the IEEE/CVF conference on computer vision and pattern recognition*, 2021, pp. 8575–8584.
- [18] M. Gholami, B. Wandt, H. Rhodin, R. Ward, and Z. J. Wang, "Adapt-pose: Cross-dataset adaptation for 3d human pose estimation by learnable motion generation," in *Proceedings of the IEEE/CVF Conference on Computer Vision and Pattern Recognition*, 2022, pp. 13 075–13 085.
- [19] Q. Peng, C. Zheng, and C. Chen, "Source-free domain adaptive human pose estimation," in *Proceedings of the IEEE/CVF International Conference on Computer Vision*, 2023, pp. 4826–4836.
- [20] —, "A dual-augmentor framework for domain generalization in 3d human pose estimation," in *Proceedings of the IEEE/CVF Conference on Computer Vision and Pattern Recognition*, 2024, pp. 2240–2249.
- [21] W. Chai, Z. Jiang, J.-N. Hwang, and G. Wang, "Global adaptation meets local generalization: Unsupervised domain adaptation for 3d human pose estimation," in *Proceedings of the IEEE/CVF International Conference on Computer Vision*, 2023, pp. 14 655–14 665.
- [22] H. Liu, J.-Y. He, Z.-Q. Cheng, W. Xiang, Q. Yang, W. Chai, G. Wang, X. Bao, B. Luo, Y. Geng *et al.*, "Posynda: Multi-hypothesis pose synthesis domain adaptation for robust 3d human pose estimation," in *Proceedings of the 31st ACM International Conference on Multimedia*, 2023, pp. 5542–5551.
- [23] D. Pavllo, C. Feichtenhofer, D. Grangier, and M. Auli, "3d human pose estimation in video with temporal convolutions and semi-supervised training," in *Proceedings of the IEEE/CVF conference on computer vision and pattern recognition*, 2019, pp. 7753–7762.
- [24] J. Zhang, Z. Tu, J. Yang, Y. Chen, and J. Yuan, "Mixste: Seq2seq mixed spatio-temporal encoder for 3d human pose estimation in video," in *Proceedings of the IEEE/CVF conference on computer vision and pattern recognition*, 2022, pp. 13 232–13 242.
- [25] K. Lin, L. Wang, and Z. Liu, "End-to-end human pose and mesh reconstruction with transformers," in *Proceedings of the IEEE/CVF conference on computer vision and pattern recognition*, 2021, pp. 1954–1963.
- [26] L. Jin, C. Xu, X. Wang, Y. Xiao, Y. Guo, X. Nie, and J. Zhao, "Single-stage is enough: Multi-person absolute 3d pose estimation," in *Proceedings of the IEEE/CVF Conference on Computer Vision and Pattern Recognition*, 2022, pp. 13 086–13 095.
- [27] J. Li, S. Bian, Q. Liu, J. Tang, F. Wang, and C. Lu, "Niki: Neural inverse kinematics with invertible neural networks for 3d human pose and shape estimation," in *Proceedings of the IEEE/CVF Conference on Computer Vision and Pattern Recognition*, 2023, pp. 12 933–12 942.
- [28] I. Sáradi, A. Hermans, and B. Leibe, "Learning 3d human pose estimation from dozens of datasets using a geometry-aware autoencoder to bridge between skeleton formats," in *Proceedings of the IEEE/CVF Winter Conference on Applications of Computer Vision*, 2023, pp. 2956–2966.
- [29] C. Zheng, S. Zhu, M. Mendieta, T. Yang, C. Chen, and Z. Ding, "3d human pose estimation with spatial and temporal transformers," in *Proceedings of the IEEE/CVF international conference on computer vision*, 2021, pp. 11 656–11 665.
- [30] Z. Zou and W. Tang, "Modulated graph convolutional network for 3d human pose estimation," in *Proceedings of the IEEE/CVF international conference on computer vision*, 2021, pp. 11 477–11 487.
- [31] W. Li, H. Liu, H. Tang, P. Wang, and L. Van Gool, "Mhformer: Multi-hypothesis transformer for 3d human pose estimation," in *Proceedings of the IEEE/CVF Conference on Computer Vision and Pattern Recognition*, 2022, pp. 13 147–13 156.
- [32] Z. Tang, Z. Qiu, Y. Hao, R. Hong, and T. Yao, "3d human pose estimation with spatio-temporal criss-cross attention," in *Proceedings of the IEEE/CVF Conference on Computer Vision and Pattern Recognition*, 2023, pp. 4790–4799.
- [33] K. Sun, B. Xiao, D. Liu, and J. Wang, "Deep high-resolution representation learning for human pose estimation," in *Proceedings of the IEEE/CVF conference on computer vision and pattern recognition*, 2019, pp. 5693–5703.
- [34] S. Li, L. Ke, K. Pratama, Y.-W. Tai, C.-K. Tang, and K.-T. Cheng, "Cascaded deep monocular 3d human pose estimation with evolutionary training data," in *Proceedings of the IEEE/CVF conference on computer vision and pattern recognition*, 2020, pp. 6173–6183.
- [35] S. Jin, L. Xu, J. Xu, C. Wang, W. Liu, C. Qian, W. Ouyang, and P. Luo, "Whole-body human pose estimation in the wild," in *Computer Vision—ECCV 2020: 16th European Conference, Glasgow, UK, August 23–28, 2020, Proceedings, Part IX 16*. Springer, 2020, pp. 196–214.
- [36] J. Martinez, R. Hossain, J. Romero, and J. J. Little, "A simple yet effective baseline for 3d human pose estimation," in *Proceedings of the IEEE international conference on computer vision*, 2017, pp. 2640–2649.
- [37] H.-S. Fang, J. Li, H. Tang, C. Xu, H. Zhu, Y. Xiu, Y.-L. Li, and C. Lu, "Alphapose: Whole-body regional multi-person pose estimation and tracking in real-time," *IEEE Transactions on Pattern Analysis and Machine Intelligence*, vol. 45, no. 6, pp. 7157–7173, 2022.
- [38] P. Lu, T. Jiang, Y. Li, X. Li, K. Chen, and W. Yang, "Rtmo: Towards high-performance one-stage real-time multi-person pose estimation," in *Proceedings of the IEEE/CVF Conference on Computer Vision and Pattern Recognition*, 2024, pp. 1491–1500.
- [39] S. Liu, X. Xie, and G. Shi, "Human pose estimation via parse graph of body structure," *IEEE Transactions on Circuits and Systems for Video Technology*, 2024.
- [40] W. Shan, Z. Liu, X. Zhang, Z. Wang, K. Han, S. Wang, S. Ma, and W. Gao, "Diffusion-based 3d human pose estimation with multi-hypothesis aggregation," in *Proceedings of the IEEE/CVF International Conference on Computer Vision*, 2023, pp. 14 761–14 771.
- [41] Q. Cai, X. Hu, S. Hou, Y. Li, and Y. Huang, "Disentangled diffusion-based 3d human pose estimation with hierarchical spatial and temporal denoiser," in *Proceedings of the AAAI Conference on Artificial Intelligence*, 2024, pp. 882–890.
- [42] G. Rogez and C. Schmid, "Mocap-guided data augmentation for 3d pose estimation in the wild," *Advances in neural information processing systems*, vol. 29, 2016.
- [43] D. Mehta, S. Sridhar, O. Sotnychenko, H. Rhodin, M. Shafiee, H.-P. Seidel, W. Xu, D. Casas, and C. Theobalt, "Vnect: Real-time 3d human pose estimation with a single rgb camera," *Acm transactions on graphics (tog)*, vol. 36, no. 4, pp. 1–14, 2017.
- [44] Y. Xu, W. Wang, T. Liu, X. Liu, J. Xie, and S.-C. Zhu, "Monocular 3d pose estimation via pose grammar and data augmentation," *IEEE transactions on pattern analysis and machine intelligence*, vol. 44, no. 10, pp. 6327–6344, 2021.
- [45] C.-Y. Yang, J. Luo, L. Xia, Y. Sun, N. Qiao, K. Zhang, Z. Jiang, J.-N. Hwang, and C.-H. Kuo, "Camerapose: Weakly-supervised monocular 3d human pose estimation by leveraging in-the-wild 2d annotations," in *Proceedings of the IEEE/CVF Winter Conference on Applications of Computer Vision*, 2023, pp. 2924–2933.
- [46] S. Du, Z. Yuan, P. Lai, and T. Ikenaga, "Joypose: Jointly learning evolutionary data augmentation and anatomy-aware global-local representation for 3d human pose estimation," *Pattern Recognition*, vol. 147, p. 110116, 2024.
- [47] J.-H. Kim and S.-W. Lee, "Toward approaches to scalability in 3d human pose estimation," in *The Thirty-eighth Annual Conference on Neural Information Processing Systems*, 2024.
- [48] S. Guan, J. Xu, Y. Wang, B. Ni, and X. Yang, "Bilevel online adaptation for out-of-domain human mesh reconstruction," in *Proceedings of the IEEE/CVF Conference on Computer Vision and Pattern Recognition*, 2021, pp. 10 472–10 481.
- [49] B. Wandt and B. Rosenhahn, "Repnet: Weakly supervised training of an adversarial reprojection network for 3d human pose estimation," in *Proceedings of the IEEE/CVF conference on computer vision and pattern recognition*, 2019, pp. 7782–7791.

- [50] B. Wandt, H. Ackermann, and B. Rosenhahn, "A kinematic chain space for monocular motion capture," in *Proceedings of the European Conference on Computer Vision (ECCV) Workshops*, 2018, pp. 0–0.
- [51] X. Mao, Q. Li, H. Xie, R. Y. Lau, Z. Wang, and S. Paul Smolley, "Least squares generative adversarial networks," in *Proceedings of the IEEE international conference on computer vision*, 2017, pp. 2794–2802.
- [52] T. Von Marcard, R. Henschel, M. J. Black, B. Rosenhahn, and G. Pons-Moll, "Recovering accurate 3d human pose in the wild using imus and a moving camera," in *Proceedings of the European conference on computer vision (ECCV)*, 2018, pp. 601–617.
- [53] C. Ionescu, D. Papava, V. Olaru, and C. Sminchisescu, "Human3.6m: Large scale datasets and predictive methods for 3d human sensing in natural environments," *IEEE transactions on pattern analysis and machine intelligence*, vol. 36, no. 7, pp. 1325–1339, 2013.
- [54] N. Kolotouros, G. Pavlakos, M. J. Black, and K. Daniilidis, "Learning to reconstruct 3d human pose and shape via model-fitting in the loop," in *Proceedings of the IEEE/CVF international conference on computer vision*, 2019, pp. 2252–2261.
- [55] M. Kocabas, N. Athanasiou, and M. J. Black, "Vibe: Video inference for human body pose and shape estimation," in *Proceedings of the IEEE/CVF conference on computer vision and pattern recognition*, 2020, pp. 5253–5263.
- [56] K. Lin, L. Wang, and Z. Liu, "Mesh graphormer," in *Proceedings of the IEEE/CVF international conference on computer vision*, 2021, pp. 12939–12948.

BIOGRAPHY SECTION

Jingjing Liu received the Ph.D degree from the School of Mechanical Engineering, Shanghai Jiao Tong University, Shanghai, China, in 2023. She is currently a research associate in University of Bristol, the United Kingdom. Her current research interests include computer vision, human activity recognition, pose estimation and applications in parkinson's monitoring.

Zhiyong Wang (Member, IEEE) received the Ph.D. degree in mechanical engineering from the School of Mechanical Engineering, Shanghai Jiao Tong University, Shanghai, China, in 2023. He is currently an Assistant Professor with the Harbin Institute of Technology Shenzhen, Shenzhen, China. His research interests include human-computer interaction, brain functional response, gaze estimation, and their practical applications in medical rehabilitation.

Xinyu Fan is currently working toward the undergraduate degree in automation from Xiamen University, Fujian, China. His research interests include computer vision, deep learning, human pose estimation and 3D reconstruction.

Amirhossein Dadashzadeh is a Research Associate in Computer Vision at the University of Bristol. He holds a Ph.D. in Computer Science from the same institution. His research focuses on developing advanced algorithms for monitoring Parkinson's patients by analysing human actions in video data.

Honghai Liu (Fellow, IEEE) received the Ph.D. degree in robotics from King's College London, London, U.K., in 2003. He is currently a Professor with the School of Mechanical Engineering and Automation, Harbin Institute of Technology Shenzhen, Shenzhen, China, and with the School of Computing, Portsmouth, U.K. His research interests include human-machine interaction, computer vision, machine learning and their clinical applications with an emphasis on approaches that could make contribution to the intelligent connection of perception to action using contextual information. Prof. Liu was a member of European Academy of Sciences. He is an Associate Editor of IEEE TRANSACTIONS ON INDUSTRIAL CYBERNETICS and the Coeditors-in-Chief of IEEE TRANSACTIONS ON INDUSTRIAL INFORMATICS.

Majid Mirmehdi is a Professor of Computer Vision in the School of Computer Science at the University of Bristol. His research interests include natural scene analysis, healthcare monitoring using vision and other sensors, and human and animal motion and behaviour understanding. He has more than 250 refereed journal and conference publications in these and other areas. MM is a Fellow of the International Association for Pattern Recognition and a Distinguished Fellow of the British Machine Vision Association. He is Editor-in-Chief of IET Computer Vision journal and an Associate Editor of Pattern Recognition journal. He is a member of the IET and serves on the Executive Committee of the British Machine Vision Association.